Supplemental Figures

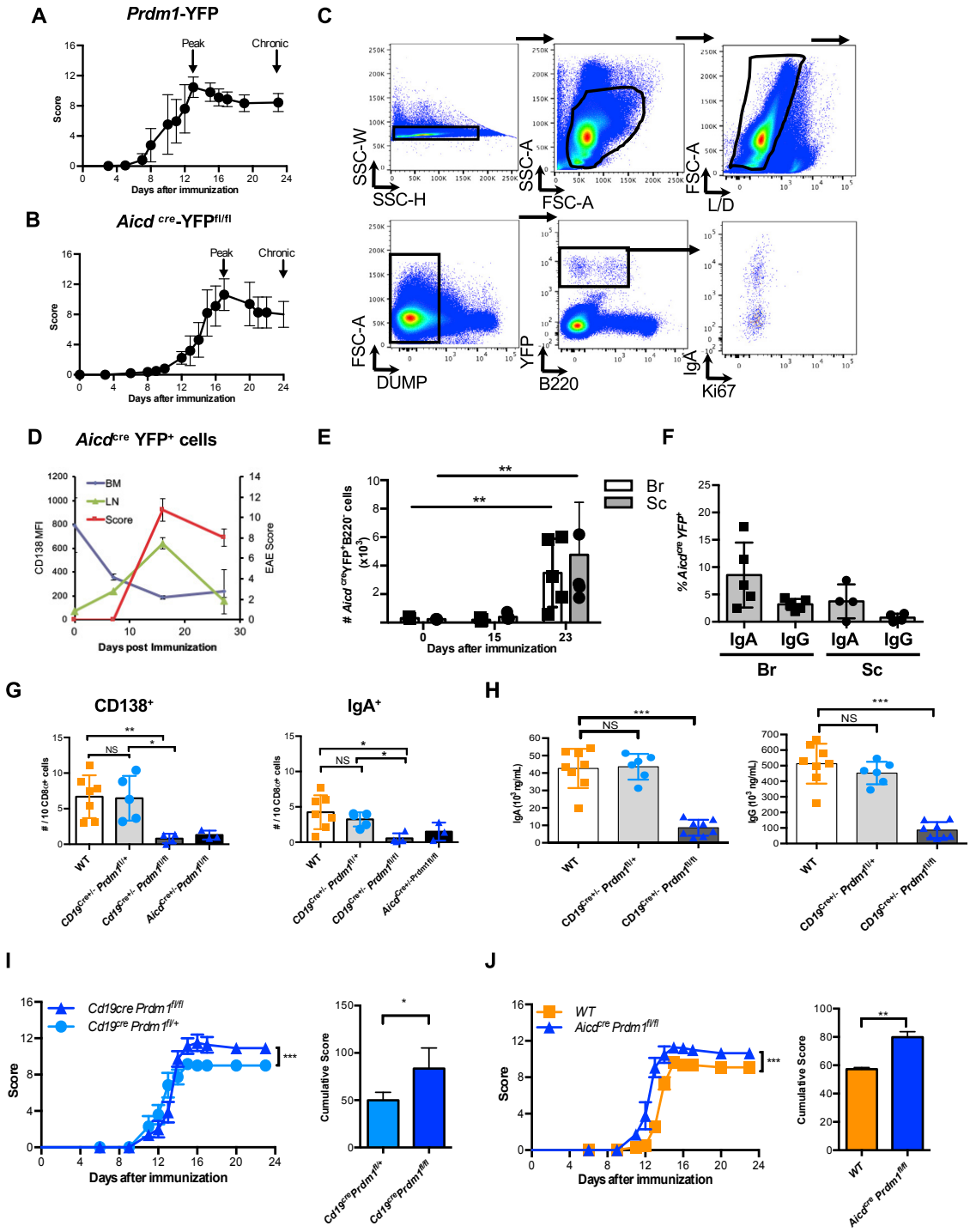

Figure S1. Quantifying CNS-Resident PB and/or PC and Assessing Their Role in EAE, Related to Figure 1

(A and B) (A) Clinical course of EAE for *Prdm1*^{cre}-YFP$^{fl/fl}$ and (B) *Aicd*^{cre}-YFP$^{fl/fl}$ mice.

(C) Flow cytometry gating strategy used to analyze PB and/or PC (see STAR Methods for details on Dump gate).

(D) Median fluorescence intensity (MFI) of CD138 after gating on YFP^{+}B220$^{int/-}$ PB and/or PC cells in BM (blue) and LN (green) during EAE (clinical score depicted in red) in *Aicd*^{cre}-YFP$^{fl/fl}$ mice.

(E) Absolute numbers of YFP^{+}B220$^{int/-}$ PB and/or PC in the Br and Sc of *Aicd*^{cre}-YFP$^{fl/fl}$ mice at different time points during EAE.

(F) Frequencies of cells expressing IgA or IgG (intracellular) expressed as a percentage of total of YFP^{+} cells in both Br and Sc of *Aicd*^{cre}-YFP$^{fl/fl}$ mice.

(G) Confirmation of PC ablation in *Cd19*^{cre}*Pdrm1*$^{fl/fl}$ mice compared to littermate controls by immunfluorescence microscopy quantification of CD138^{+} (left) or IgA^{+} PC (right) in the SILP using CD8α as a normalizing denominator.

(legend continued on next page)

(H) Confirmation of PC ablation in *Cd19*^{cre}*Pdrm1*$^{fl/fl}$ mice compared to littermate controls by measuring levels of IgA (left) or IgG (right) in the serum by ELISA.
(I) EAE clinical scores for *Cd19*$^{-cre}$ *Prdm1*$^{fl/fl}$ *versus Cd19*$^{-cre}$*Prdm1*$^{fl/+}$ littermates.
(J) EAE clinical scores for *Aicd*^{cre}*Prdm1*$^{fl/fl}$ versus WT mice.
Experiments (A,B,D,I,J) were repeated 3 times with at least 5 mice per group per experiment. Experiment (E,F) was performed 5 times with 4-5 mice per group per experiment. Experiment (G-H) was repeated twice with 5-8 mice per group per experiment. Experiment (I-J) were performed on 5-6 mice per group. * = $p < 0.05$, **$p < 0.01$, ***$p < 0.001$. Two-way ANOVA Test and Mann Whitney Test. Mean and SEM.

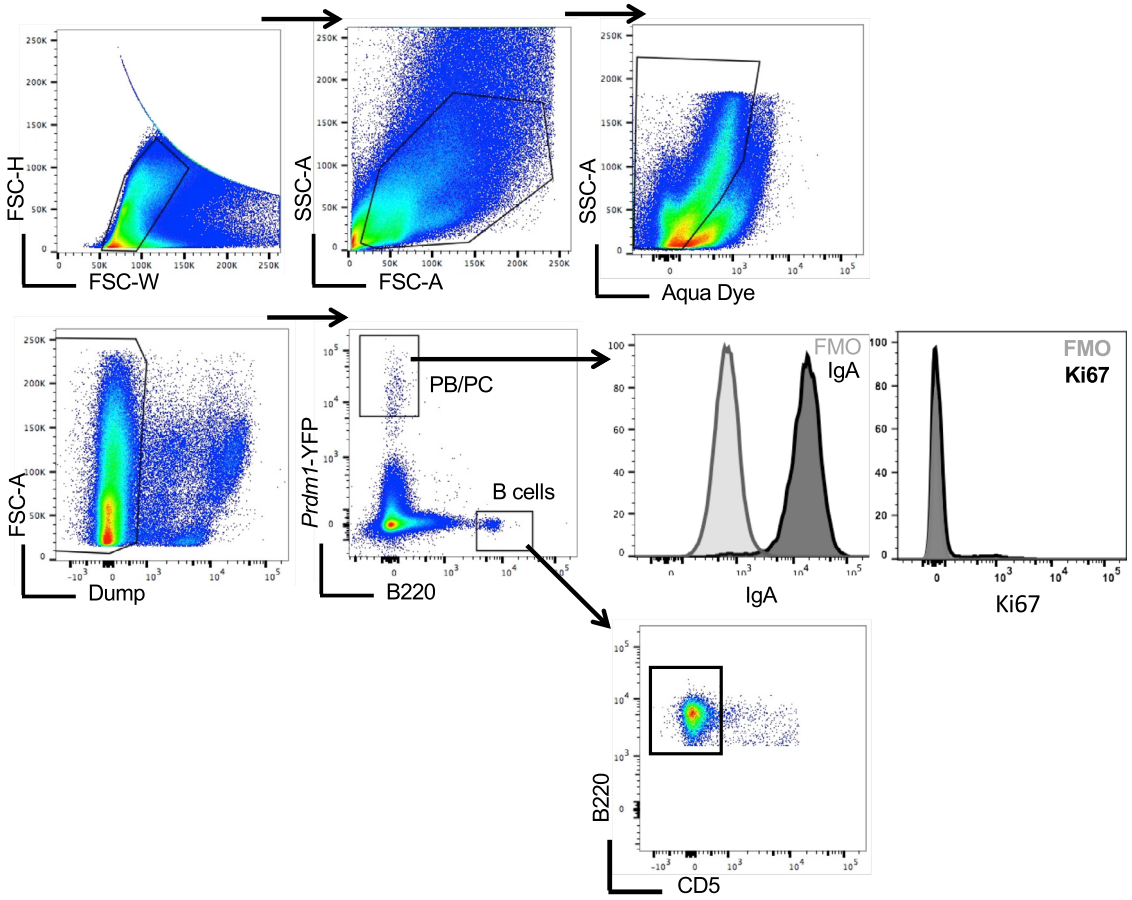

Figure S2. Post-Sort Analysis of Gut PB and/or PC Prior to Adoptive Transfer, Related to Figure 2

Gating strategy for sorting gut PC versus gut B cells. Post-sort analysis demonstrated 96%–98% purity with the majority of transferred cells expressing intracellular IgA and staining negative for Ki67 and B220. Please see STAR Methods for Dump gate.

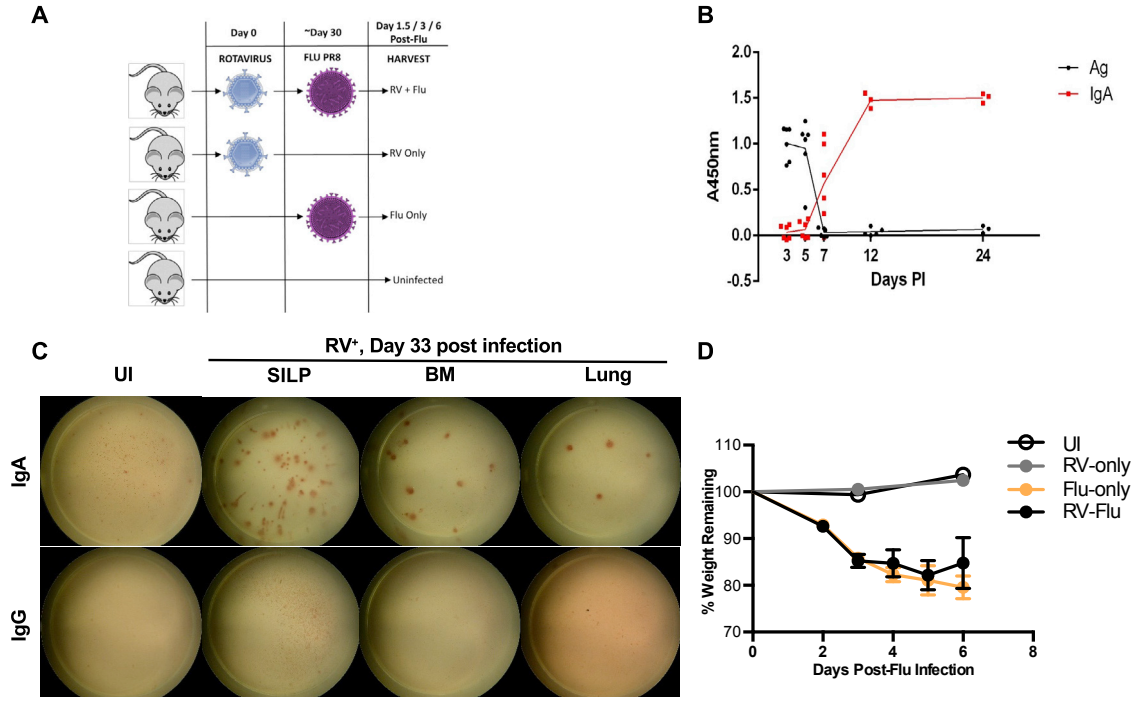

Figure S3. Using Rotavirus Infection to Track Intestinal B Cells, Related to Figure 3

(A) Schematic representation of the dual-infection model used for tracking gut-derived PB and/or PC.

(B) RV antigen (Ag) and RV-specific IgA measured by ELISA. A representative infection course is depicted.

(C) Representative RV-specific IgA ASC detected after Flu infection by ELISPOT whereby each spot is counted as one ASC.

(D) Representative disease course (% weight remaining) during flu infection for each of the groups depicted in (A). Day 6 was considered to be the end point as few mice survived beyond day 6. All harvests were performed on or before this time point. Mean and SEM depicted.

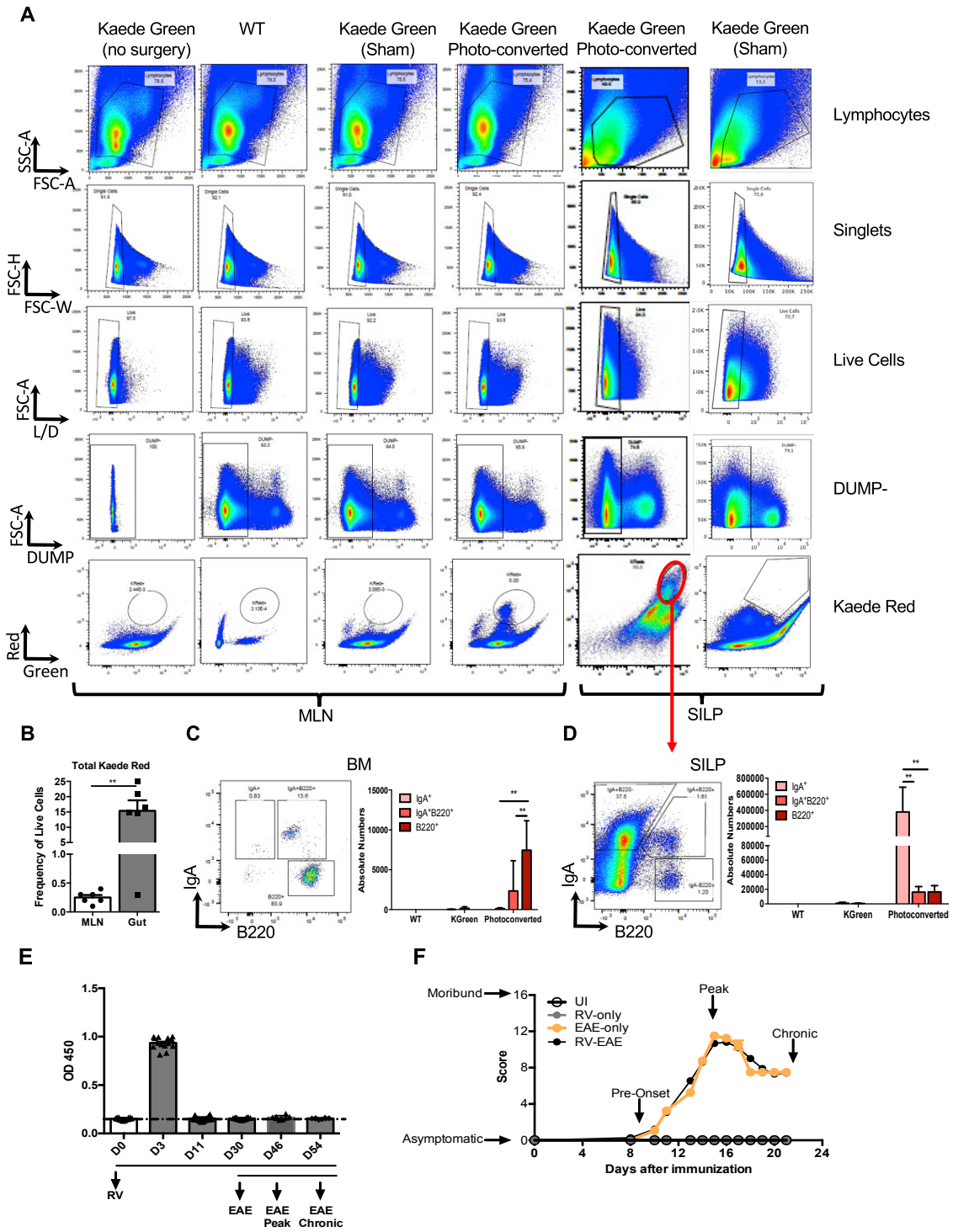

Figure S4. Using Photo-Conversion of Kaede^{+} Cells in the Small Intestine in the Steady State and Rotavirus Infection to Track Mucosal B Cell Trafficking during EAE, Related to Figures 3 and 4

(A) Gating strategy for negative controls (Kaede-green (non-photoconverted), WT and Sham-surgery mice) and photoconverted Kaede-transgenic mice for quantification of Kaede-Red (K-Red) populations in various tissues (mesenteric LN and SILP are shown), and also the analysis of IgA versus B220 derived from K-Red cells in the gut and BM. Note that gates were established for each individual tissue (due to tissue-specific autofluorescent properties) based on sham surgery controls for K-Red assessment and in the case of IgA/B220 assessment, gates were established for each individual tissue based on FMO controls.

(B) Frequency of photoconverted cells in the K-Red MLN versus SILP.

(legend continued on next page)

(C) Absolute numbers of photoconverted cells in the BM.

(D) Absolute numbers of photoconverted cells in the SILP.

(E) RV-Ag ELISA on stool samples post-RV infection at different time points.

(F) Representative clinical scores of mice with MOG_{35-55}-induced EAE. UI = uninfected. All experiments were done 3 times with at least 5 mice per group. (Mean and SEM). These experiments were repeated 3 times. Depicted is a single experiment of n = 2 WT, n = 2 non-photoconverted KGreen and n = 6 photoconverted Kaede mice. * = $p < 0.05$, ** $p < 0.01$.

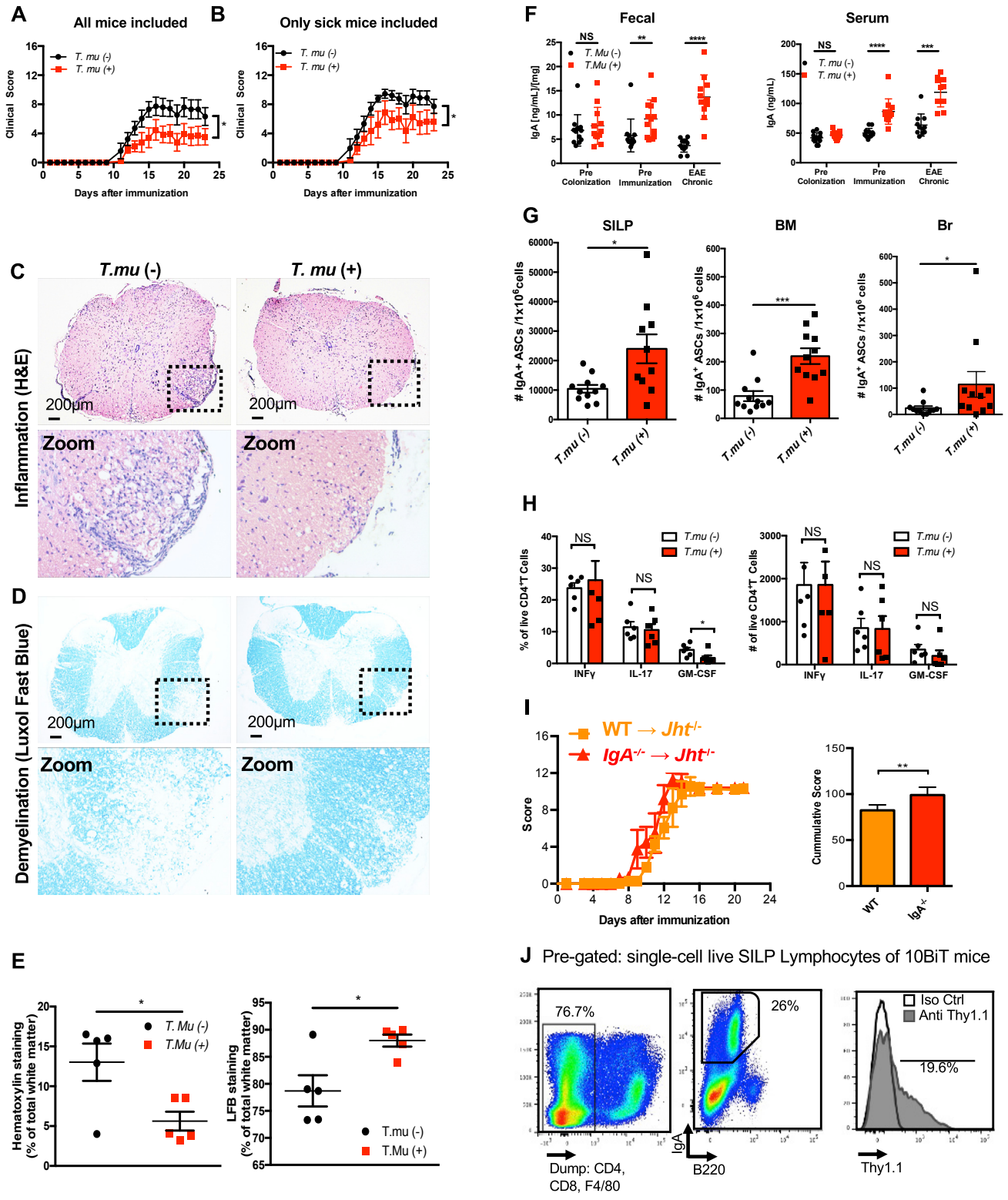

Figure S5. Colonization with *T.mu* Results in Enhanced IgA$^+$ ASC Numbers in the CNS Concomitant with Reduced EAE, however, IgA Itself Has a Limited Role in Controlling the Clinical Presentation of EAE, Related to Figure 6

(A) EAE clinical scores of WT mice colonized or not colonized with *T. mu. T.*mu+ mice harbored on average 140 × 10^6 +/− 44.9 × 10^6 trophozoites per caecum. Incidence was 9/11 *for T.mu-* and 7/11 for *T.mu+.*

(legend continued on next page)

(B) EAE clinical scores of same experiment as (A) but only sick mice are depicted, and of the mice that developed disease, average onset was day 12.4 ± 1.0 for *T.mu*- and day 14. +/− 2.4. for *T. Mu*+.
(C and D) Representative images of (C) H&E and (D) LFB staining of Sc from *T.mu* (-) and *T.mu* (+) mice harvested at the chronic phase of the disease.
(E) Quantification of H&E and LFB staining from (C) and (D).
(F) Concentration of IgA in fecal (left) and serum samples (right) collected from experiment (A).
(G) Number of Total IgA-ASC from SILP (left), BM (middle) and Br (right) during the chronic phase of EAE from experiment (A).
(H) Frequency and absolute number of cytokine producing CD4+ T cells from the Sc *T.mu*- versus *T.*mu+ mice at the chronic stage of EAE evaluated by flow cytometry.
(I) BM chimeras in which B cell deficient $Jht^{-/-}$ mice were reconstituted with WT or $IgA^{-/-}$ BM and subjected to EAE. Cumulative score is shown on the right.
(J) Representative Flow Cytometry of SILP-resident cells from 10BiT mice. Expression of Thy1.1 (which reports on the expression of *Il10* mRNA) is represented as a histogram derived from pre-gating on single cell live SILP lymphocytes from 10Bit mice.
Experiments in (A-H) were done once, n = 10 mice per group for clinical assessment of EAE and IgA measurements, then using n = 5 mice per group for histology and flow cytometry. Experiments in (I-J) were performed twice, n = 4-10 mice per group. * = $p < 0.05$, ** $p < 0.01$, *** $p < 0.001$, **** $p < 0.0001$ (Two-way ANOVA Test was performed for (A,B,I); Mann Whitney Test for (E-I). Mean and SEM shown.

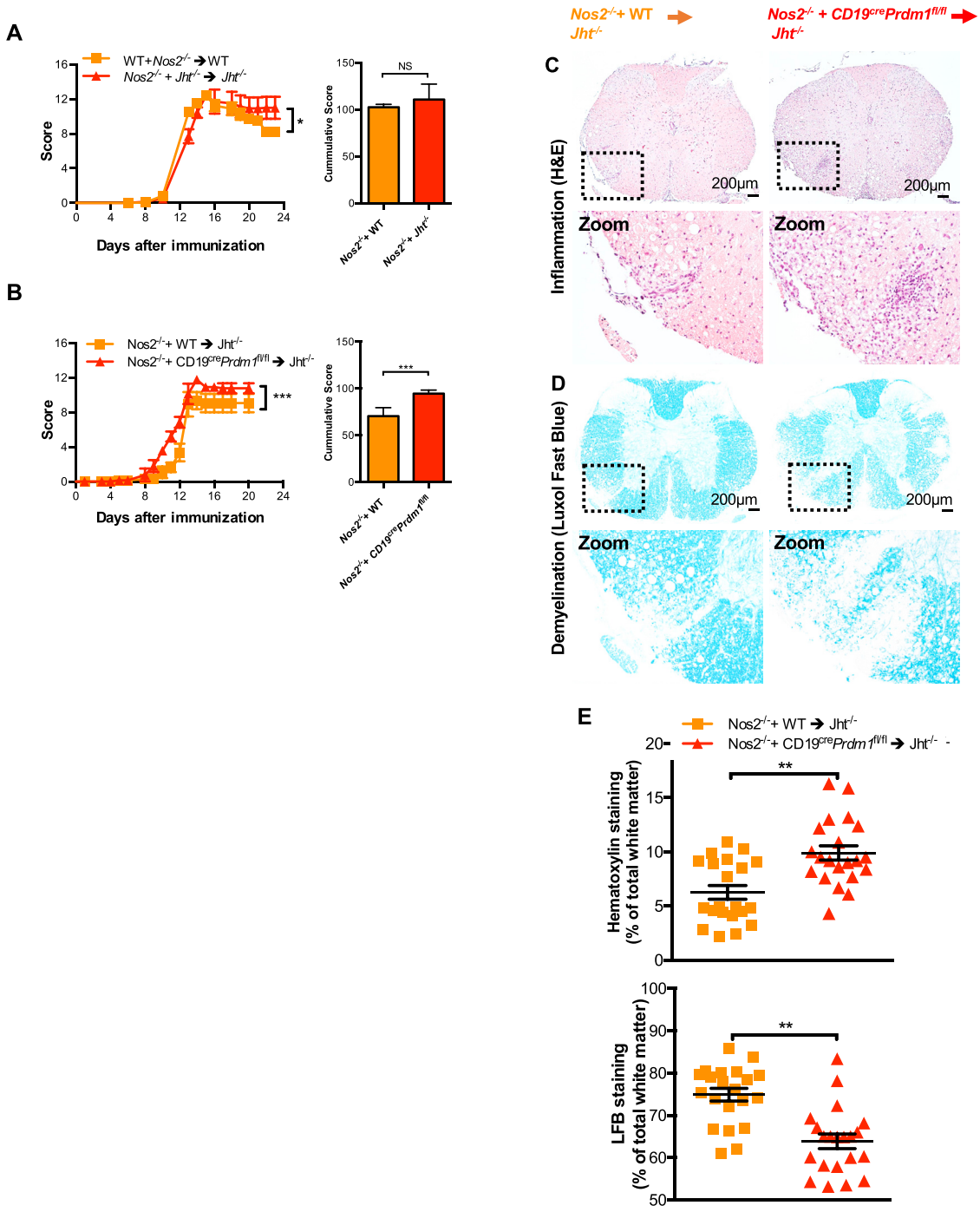

Figure S6. PB and/or PC-Intrinsic Nos2 Plays a Secondary Role in Limiting EAE Pathology, Related to Figure 6

(A) EAE clinical scores of *Nos2*$^{-/-}$ + *Jht*$^{-/-}$ → *Jht*$^{-/-}$ versus *Nos2*$^{-/-}$ + WT → *Jht*$^{-/-}$ mixed-BM chimeras, or (B) *Nos2*$^{-/-}$ + *Cd19*^{cre}*Prdm1*$^{-/-}$ → *Jht*$^{-/-}$ versus *Nos2*$^{-/-}$ + WT → *Jht*$^{-/-}$ mixed-BM chimeras. Cumulative score for (A) and (B) are shown on the right. Representative images of H&E (C) and LFB *Jht*$^{-/-}$ (D) are shown. (E) Quantification of H&E staining (Top) and LFB (Bottom) from (C-D) is shown. Experiments in (A) were done 4 times with 6-10 mice per group for each experiment and experiment in (B) was done once with n = 7 mice per group. Two-way ANOVA for (A,B) and Mann Whitney Test for (E). Mean and SEM are shown. ** = $p < 0.01$ or *** = $p < 0.001$.

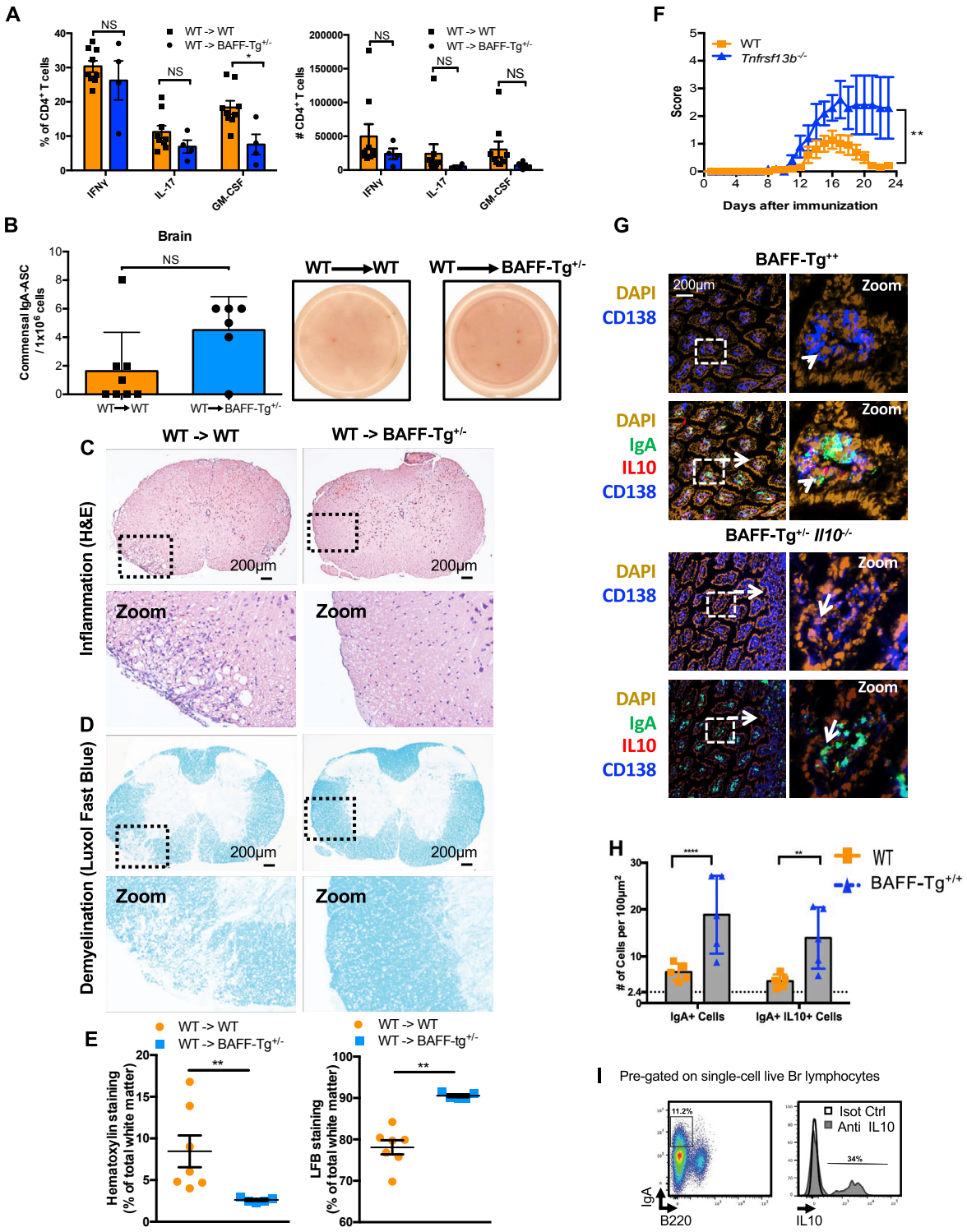

Figure S7. The Effector Phase of EAE Is Inhibited by Excess BAFF. Related to Figure 7

(A) Frequency and absolute numbers of cytokine producing CD4+ T cells from the Sc of WT and Baff-Tg mice during adoptive transfer EAE was evaluated by flow cytometry. (B) Quantification of commensal-reactive IgA ASC in the Br of WT and Baff-Tg mice after adoptive transfer EAE (as in A) by ELISPOT. Representative images of (C) H&E and (D) LFB staining from the experiment in (A). (E) Quantification of H&E staining (left) and LFB staining (right) from (C) and (D). (F) EAE Clinical Scores in WT and *Tnfrsf13b*$^{-/-}$ mice that lack TACI. WT mice are littermate controls derived from backcrosses to C57BL/6 animals at the University of Melbourne. (G) Representative immunofluoresence images of DAPI and CD138 or a merged image of IgA, IL10 and CD138 in small intestinal samples from BAFF-Tg$^{+/+}$ and

(legend continued on next page)

BAFF-Tg$^{+/-}$ x IL10$^{-/-}$ mice. Arrows in the Zoomed image of BAFF-Tg$^{+/+}$ SILP represent cells that are positive for both IgA and IL10 and arrows in the Zoomed image of BAFF-Tg$^{+/-}$ x IL10$^{-/-}$ SILP represent cells that are positive only for IgA. (H) Quantification of IgA^{+}IL10^{+} cells per 100μm^2, with the dotted line representing the number of IL10^{+} cells counted in an IL10$^{-/-}$ mouse to show the specificity of the assay. (I) Representative flow cytometry dot plots of intracellular detection of IL10 in IgA^{+}B220^{-}PB and/or PC in Baff-Tg mice. Experiments in (A-E) were done once, n = 5-6 mice per group. Experiment in (f) was done twice, 5-9 mice per group. Experiments in (G-H) were done once, n = 5 mice per group. Experiment in (I) was done twice, 6 mice per group. * = $p < 0.05$, ** $p < 0.01$, *** $p < 0.001$ (Two-way ANOVA Test for (F); Mann Whitney Test for (A, B, E, H). Mean and SEM are shown.